Hindawi
International Journal of Aerospace Engineering
Volume 2021, Article ID 8827141, 16 pages
https://doi.org/10.1155/2021/8827141

Research Article

Dynamics Modeling and Simulation of a Net Closing Mechanism for Tether-Net Capture

Jiyue Si,[1] **Zhaojun Pang**,[1] **Zhonghua Du**,[1] **and Jie Fu**[2]

[1]*School of Mechanical Engineering, Nanjing University of Science and Technology, 210094 Nanjing, China*
[2]*Shanghai Academy of Spaceflight Technology, Shanghai 201109, China*

Correspondence should be addressed to Zhaojun Pang; pangzj@njust.edu.cn

Received 30 May 2020; Revised 18 December 2020; Accepted 19 December 2020; Published 4 January 2021

Academic Editor: Enrico C. Lorenzini

Tether-net is a promising active debris removal technique, and a closing mechanism can ensure the reliable wrapping of space debris by using tether-net. This study focuses on the dynamics model of the split closing mechanism and the sliding joint between thread and ring. First, a new kind of closing mechanism is proposed, which drives the closing thread to close the net mouth through the split masses, and the mass-spring-damper method is used to model tether-net. Thereafter, for the first time, the model of thread-ring sliding joint is proposed based on the mass-spring-damper method, which can be used to simulate the closing process of tether-net. Finally, one-edge closure experiment of the net is carried out and the experimental results are compared with the simulation results, and the closing process of the tether-net is simulated by using the thread-ring sliding joint. Results reveal that the thread-ring sliding joint can be used to simulate the relative slip between the thread and the ring, and the tether-net can wrap the target reliably in a short time by using the split closing system. The split closing mechanism can make it possible for the tether-net to close successfully, whether it starts to work before or after the net contacts with the target.

1. Introduction

Since the beginning of space activities, the number of space debris has remarkably increased, and space debris may threaten critical space infrastructure, such as the International Space Station [1]. Tether-net is a new kind of active debris removal (ADR) technique, which is flexible, lightweighted, and cost-efficient [2, 3].

The capture task of tether-net system includes three main phases: deployment stage of the net, collision stage between the net and the target, and reliable closing stage of the net [4]. The first two stages have attracted much attention. Benvenuto et al. discretized the net via the mass-spring-damper method and the studied capture of a full-scale tumbling target [5]. Shan et al. modeled the tether-net by the absolute nodal coordinate formulation (ANCF) and the mass-spring-damper method [6, 7], and an impulse-based method was used in a net capturing scenario [8]. Botta et al. evaluated the effect of different contact force models on the capture results, and a modified damped bristle model for the friction force is chosen [9, 10]. Si et al. studied the dynamics model of the self-collision of tether-net, and a line–line self-collision detection algorithm is proposed according to the geometric characteristics of tether-net [4]. Scholars and institutions performed experiments on the deployment and collision phase of tether-net, including the capture test in 0 g environment and the net drop test, which verify the feasibility of tether-net in ADR [11–13]. Zhang and Huang installed thrusters on the bullets to control the net and improve capture performance of net [14, 15].

To ensure the reliable wrapping of target by tether-net, the net mouth can be closed by using the closing system after the net contacts with the target. According to the storage method of the closing thread, the closing mechanism can be divided into internal storage and external storage. The internal storage closing mechanism stores the closing thread inside the closing mechanism and generally uses small motors or springs as the power to drive the closing reel to rotate. During the closure, the closing thread is wound by closing reel inside the closing mechanism. At the same time, the area of the net mouth will be reduced, and finally, a reliable wrapping will be formed for the target [13, 16, 17]. The

external storage closing mechanism does not store the closing thread inside the closing mechanism. After the closure, the closing thread may be exposed to the space environment [18, 19]. Therefore, the space utilization rate of the external storage closing mechanism is higher. Benvenuto et al. proposed a closing mechanism using a couple of counter-rotating reels to avoid torque effects on the closing mechanism. Moreover, the closing process of planar net and pyramidal net is studied [5, 16]. Zhai and Zhang connected the net and bullets through threshold linkers, which detect a tension between the net and the bullets. The bullets will disconnect from the net when tension reaches the threshold. After the bullets lose the restraint of the threshold linkers, the closing thread drove by the bullets to closing the net mouth under the action of inertia [18]. Sharf et al. proposed a tether-actuated cinch-cord mechanism for closing net around debris. The performance of the mechanism was verified by ground test, and the process of net closure was simulated in the space environment [19]. Botta et al. established the model of the winch based on their previous work. Two control laws for the winch velocity during deployment and closure of the net, respectively, are formulated and tested in simulation [20].

In the above research, to close the net mouth, the closing thread and the ring must slip relatively. Therefore, the establishment of the thread-ring sliding joint is the core issue of the numerical simulation of the closing process of a net. The literature mentioned above focuses on the closing method discussion, but these studies do not provide the dynamics model of the net closure. Research on the sliding joint is mostly concentrated in the field of rail transit. The modeling methods used include the finite element method and ANCF [21–23]. Shabana proposes ANCF based on the finite element method and continuum mechanics theory [24, 25], which can be used to solve large deformation and displacement of flexible multibody dynamics problems. The lower order cable element can be used in the simulation of tether-net [6, 26], but ANCF has more degrees of freedom. Moreover, its calculation efficiency is much lower than that of the mass-spring-damper method. In the cosimulation of deployment, collision, and closure, the computational cost will be enormous. Therefore, an efficient sliding model based on the mass-spring-damper method is necessary. The internal storage closing mechanism stores the closing thread inside the mechanism and needs to reserve the space for the closing thread. The volume of the mechanism is generally large, which is especially evident when the net is large. Therefore, a type of external storage closing mechanism is proposed in this study. The mechanism can launch two split masses through spring or high-pressure gas, which drive the closing thread to close the net mouth. Moreover, a thread-ring slipping joint based on the mass-spring-damper method is proposed to simulate the closing process of the net.

This study consists of six parts. Section 2 proposes a new kind of split closing mechanism. Section 3 introduces the geometric configuration and dynamics model of tether-net. Section 4 proposes a thread-ring slipping model based on the mass-spring-damper method. Section 5 discusses the simulations and experiments of the closing process of a net. Section 6 summarizes the work.

2. Split Closing Mechanism

In the ADR mission, the net may be hooked with protrusions of the target during capture, and the bullets may also intertwine with the net. The twining may not occur in every scenario, and even if such twining occurs, it may fail at a specific time. The wrapping of debris is not reliable because the surface of the debris may be smooth, and the debris may be rotating. Therefore, to make a reliable wrapping of target by tether-net, the closing mechanism is critical in the ADR mission. For the conceptual design of a tether-net closing mechanism, a solution is desired, which would be simple, cost-effective, nonintrusive, and highly reliable [19]. Moreover, the mechanism should work independently of the chaser spacecraft to improve the reliability of the closing mechanism.

Therefore, a split closing system is proposed in this study. The closing system is composed of four parts: split closing mechanism, ring, one-way locking mechanism, and closing thread, as shown in Figure 1. One split closing mechanism is composed of two split masses and a launcher. The two split masses have the same mass and are connected with different closing threads. The launcher is attached with the towing thread of the net, and a time-delay switch is installed inside it. The starting time of closing of tether-net can be set by the time-delay switch. The launcher is powered by spring or high-pressure gas. When the starting time of closing is reached, the time-delay switch releases the spring or gas and the launcher shoots out the split masses along the axial direction of the closing mechanism. The number of rings connected to the edge of the net can be adjusted according to the net size. The closing system consists of eight one-way locking mechanisms connected to the edge of the net, which allow only a one-way passage of the closing thread to prevent the net opening again after closed. The closing system consists of four closing threads that pass through the rings and the one-way locking mechanisms, and the ends of the closing threads are connected to different split masses.

The sliding direction of the one-way locking mechanism relative to the closing thread is shown by the red arrow in Figure 2, where "×" indicates the direction that the one-way locking mechanism cannot slide to. During the deployment, the towing thread is in the tension state, while the closing thread is in a relaxed state. The closing thread will not slide relative to the net edge, and the one-way locking mechanism will not work or cause problems during deployment. During the closure, the rings slide toward the middle point of the closing thread, and the one-way locking mechanisms act as the rings. After the closure, the one-way locking mechanism will work only if there is a reopen tendency of the net.

After the net launched from chaser spacecraft, the time-delay switch begins to work, and the net is gradually deployed and flies toward the target at the same. The starting time of closing refers to the moment when the split closing mechanisms start to work. When the starting time of closing is reached, each launcher will shoot out two split masses. The arrow in Figure 1 shows the shooting direction. Then, with the pull of the detached masses, the rings and one-way locking mechanisms move relative to the closing thread, and the

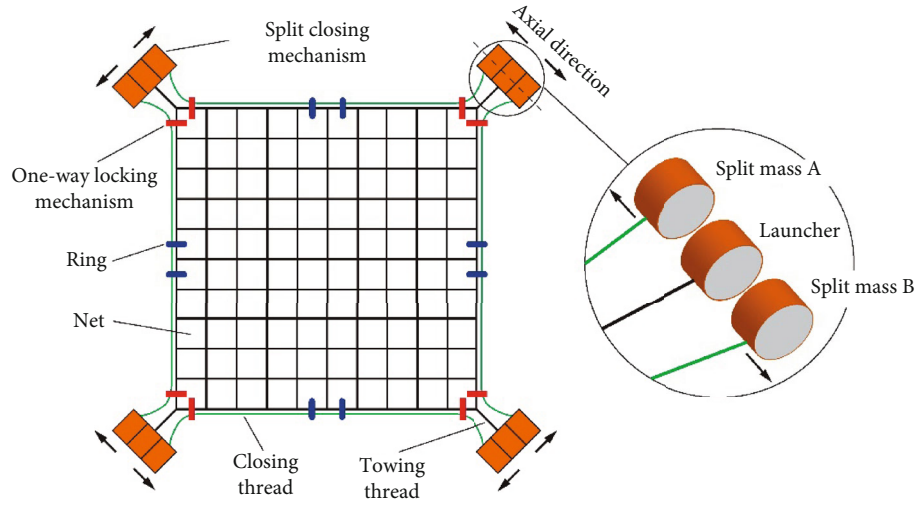

Figure 1: Split closing system.

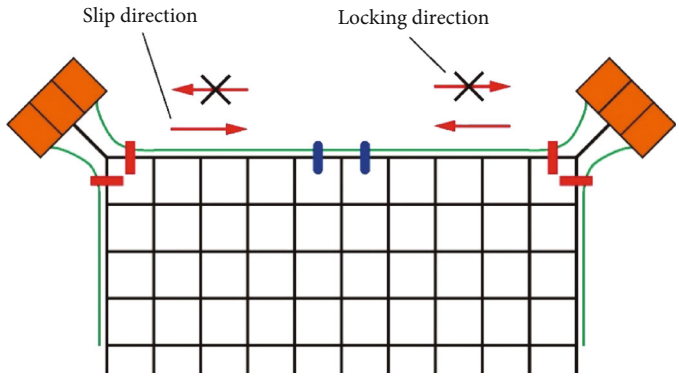

Figure 2: Sliding direction of one-way locking mechanism.

net mouth is gradually closed. The launchers move toward the center of the net with the pull of towing threads, and Figure 3 shows the status of the tether-net after the beginning of closing. The starting time of closing is related to many factors, such as net configuration, closing speed, and target state.

At present, the most common closing mechanism is internal storage type. It has the advantages of simple principle and easy implementation. However, since the closing thread is stored in the closing mechanism, the mass and volume of the closing mechanism are very large, especially when the torsional spring is used as the power. At the same time, the speed of the reels of this type of closing mechanism may not be synchronous during the closure, and the phenomenon of torque imbalance cannot be avoided completely. Another type of closing system is proposed by Sharf et al. [19]. Their design is to actuate the closure by towing the control thread connecting the chaser spacecraft to the net. However, it adds the complexity of the closure and enhances the risk of twining between the control thread and the main thread.

In the scheme of this study, one obvious advantage is that it does not have to store the closing threads in the closing mechanism. Hence, the volume of the mechanism can be reduced. The time-delay switches start immediately after the net is flung from the chaser spacecraft. The entire closing process does not need control from chaser spacecraft, which reduces the complexity of the system. The mass and separation speed of the two split masses are the same. According to the momentum conservation law, the movement state of the launcher will not change suddenly at the moment of separation and will also not affect the dynamics of the net. The closing threads in this design do not pass through the inner of the closing mechanism, which can simplify the structure of the mechanism and avoids the torque imbalance phenomenon described in Ref. [5]. The launching power can be selected according to the size of the tether-net. When the net is small, the separation speed is low, and the spring can be selected as the launching power. When the net is large, high-pressure gas can be selected as launching power.

3. Dynamics Model of Tether-Net

In this study, a square net with square mesh is studied, as shown in Figure 4. Four closing mechanisms are connected to the corners of the square net through the towing threads in turn. The one-way locking mechanisms and the rings are connected to the net edge and fixed in the middle of two physical knots (nodes) of the net edge. The one-way locking mechanism is replaced by the ring in the following sections,

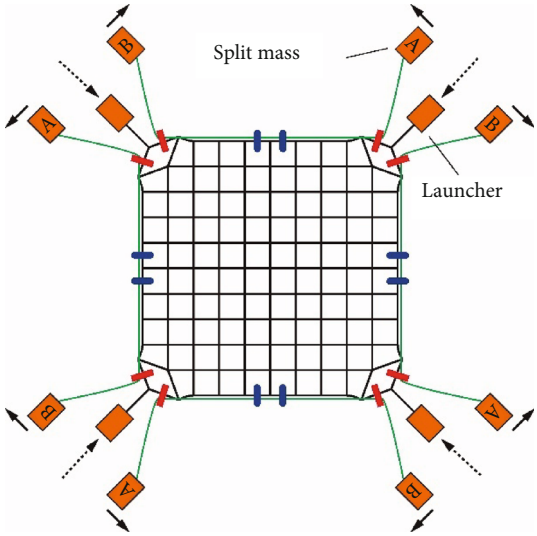

Figure 3: The tether-net after the beginning of closing.

to simplify the model. The mass-spring-damper model is used to model tether-net to lump the mass of the net in its nodes, and the threads are represented by massless spring-damper elements in parallel (shown as nodes i and j in Figure 4). The closing thread is also modeled using the mass-spring-damper model. Four closing mechanisms and 16 rings are numbered, and the two split masses of the closing mechanisms are denoted as split masses A and B, respectively.

According to Newton's second law, the dynamics equation of the i -th node, as illustrated in Figure 4 can be described as follows:

$$m_i \ddot{\boldsymbol{x}}_i = \boldsymbol{F}_{\text{int},i} + \boldsymbol{F}_{\text{ext},i}, \tag{1}$$

where m_i is the mass of the i -th node. According to the position of the i -th node in the net, m_i can be expressed as follows:

$$m_i = \begin{cases} \dfrac{m_{\text{t}}}{2} + m_{\text{c}}, & i \text{ is closing mechanism,} \\ \dfrac{n_{\text{t}} m_{\text{t}} + n_{\text{r}} m_{\text{r}}}{2}, & i \text{ is adjaccent to ring,,} \\ \dfrac{n_{\text{t}} m_{\text{t}}}{2}, & i \text{ is other node,} \end{cases} \tag{2}$$

where m_{t} is the mass of a thread element, m_{c} is the mass of the closing mechanism, m_{r} is the mass of the ring, n_{t} is the number of adjacent threads connected to the i -th node, and n_{r} is the number of adjacent rings connected to the i -th node. $\ddot{\boldsymbol{x}}_i$ is the absolute acceleration of the i -th node. $\boldsymbol{F}_{\text{int},i}$ and $\boldsymbol{F}_{\text{ext},i}$ are internal forces and external forces on the i -th node, respectively. In this paper, $\boldsymbol{F}_{\text{ext},i}$ includes contact forces, gravity, and the force produced by closing mechanism. For more details about the calculation of internal forces, the reader is referred to our previous paper [4].

4. Dynamics Model of the Thread-Ring Sliding Joint

The simulation of the closing process can help designers to select the starting time and speed of closing. The establishment of the thread-ring sliding joint is the core issue of the numerical simulation of the closing process of a net. Considering that the modeling of tether-net is mostly based on the mass-spring-damper method, this section proposes a thread-ring sliding joint based on the mass-spring-damper method, including collision detection and contact response.

4.1. Collision Detection between Thread and Ring. Collision detection is used to judge whether a collision occurs and also provides a basis for the contact response. In the process of collision detection, the flexible thread is discretized into a series of nonbendable cylinders (elements) whose diameter is equal to the diameter of thread, as shown in Figure 5. The thread-ring sliding joint takes advantage of this characteristic of the mass-spring-damper method. In this study, the collision detection between the closing thread and ring is simplified to calculate the minimum distance between the cylinder and ring in three-dimensional space. When the minimum distance satisfies the collision condition, the collision between closing thread and ring is considered to occur. The mass-spring-damper method discretizes the thread into a series of nonbending elements. Thus, the thread cannot fit the curved surface of the ring completely, which is the limitation of this model. Therefore, discretizing the thread into adequate elements is necessary to ensure the relative slip between thread and ring.

To judge whether a cylinder collides with a ring, the minimum distance between the centerline of the cylinder and the centerline (circular) of the ring should be calculated first. Moreover, whether or not the minimum distance satisfies the contact condition should be judged. Scholars have formulated a method for calculating the distance from any point on a straight line to a circle in 3D space [27, 28]. The centerline of an element can be expressed in parametric as follows:

$$\boldsymbol{A}(t) = \boldsymbol{A}_1 + t\boldsymbol{M}, \tag{3}$$

where $\boldsymbol{M} = \boldsymbol{A}_2 - \boldsymbol{A}_1$, where $\boldsymbol{A}_1$ and $\boldsymbol{A}_2$ are the two endpoints of the centerline of an element. If $0 \le t \le 1$, $\boldsymbol{A}(t)$ is located between $\boldsymbol{A}_1$ and $\boldsymbol{A}_2$. A circle B (centerline of the ring), with a radius of R_{B}, and a center of $\boldsymbol{C}_{\text{B}}$ is introduced, and the unit normal vector of the circle is $\boldsymbol{N}_{\text{B}}$ (shown in Figure 5). The square of the distance between the line and the circle can be expressed as follows [22]:

$$f(t) = a_6 t^2 + a_5 t + a_4 + a_3 \sqrt{a_2 t^2 + a_1 t + a_0}, \tag{4}$$

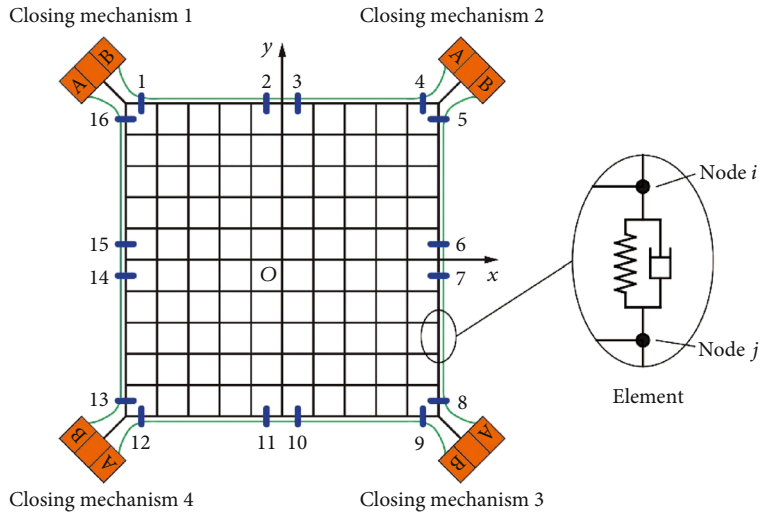

Figure 4: Configuration of the tether-net.

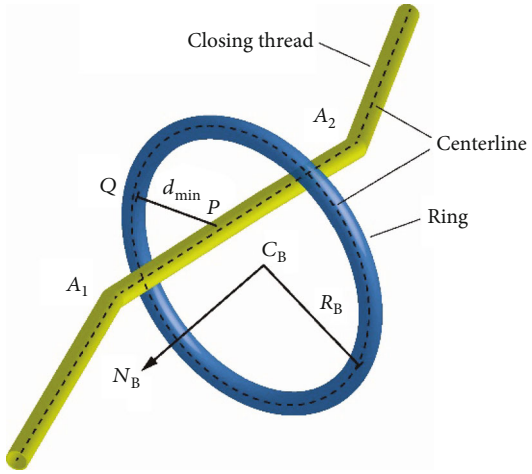

Figure 5: Discretized closing thread and ring.

where

$$\begin{cases} a_6 = \boldsymbol{M}\cdot\boldsymbol{M}, \\ a_5 = 2\boldsymbol{D}\cdot\boldsymbol{M}, \\ a_4 = \boldsymbol{D}\cdot\boldsymbol{D} + R_B^2, \\ a_3 = -2R_B^2, \\ a_2 = \boldsymbol{E}\cdot\boldsymbol{E}, \\ a_1 = 2\boldsymbol{E}\cdot\boldsymbol{F}, \\ a_0 = \boldsymbol{F}\cdot\boldsymbol{F}, \end{cases} \tag{5}$$

$$\begin{cases} \boldsymbol{D} = \boldsymbol{A}_1 - \boldsymbol{C}_B, \\ \boldsymbol{E} = \boldsymbol{M} - (\boldsymbol{N}_B\cdot\boldsymbol{M})\boldsymbol{N}_B, \\ \boldsymbol{F} = \boldsymbol{D} - (\boldsymbol{N}_B\cdot\boldsymbol{D})\boldsymbol{N}_B. \end{cases}$$

Given that no stable analytic solution is provided in Equation (7), the golden section method is used to search the minimum value of $f(t)$. The golden section method reduces the interval by the same fraction with each iteration. The intervals are derived from the golden section ratio of 1.61803. The method has provided key advantages, such as high speed convergence, easy implementation, and guaranteed convergence [29, 30].

If $0 \le t \le 1$, then, the search area is located in the segment of the element. The minimum distance of the thread and ring is $d_{min} = \min(\sqrt{f(t)})$, and r_A and r_B are the wire radii of the closing thread and ring, respectively. The collision condition of the thread and ring is $(d_{min} < r_A + r_B) \wedge (0 \le t \le 1)$.

4.2. Contact Response. The nonlinear damping model is used in this study. When collision occurs, the normal contact force is as follows [31]:

$$F = k_c\delta^n + \lambda\delta^n\dot{\delta}, \tag{6}$$

where k_c is the equivalent stiffness coefficient; δ and $\dot{\delta}$ are the penetration length and penetration rate, respectively; λ is the damping factor of contact; and n related to the contact scenario and is equal to 1.5 in this work. The expression of the above parameters can be summarized as follows [31, 32]:

$$k_c = \frac{4}{3\pi}\frac{\sqrt{r}}{h_1 + h_2}, \tag{7}$$

$$h_i = \frac{1 - \nu_i^2}{\pi E_i}, \tag{8}$$

$$\lambda = \frac{3}{2}\alpha k_c, \tag{9}$$

where r is the equivalent radius related to contact geometry. When the thread collides with the ring, the contact is simplified as the contact between two balls. The radius of the two balls is the same as the radius of the thread and the ring,

respectively. The equivalent radius of the element and ring is $r = (r_A^{-1} + r_B^{-1})^{-1}$.

When element A collides with ring B, the contact points on element and ring are defined as points P and Q, respectively. Then, the contact force of element A is found as $\boldsymbol{F}_A = -F\boldsymbol{e}_{PQ}$, where $\boldsymbol{e}_{PQ}$ is a unit vector from point P to point Q, and F can be computed from Equation (6). According to the principle of force composition and decomposition, the contact force is distributed to two endpoints of the element. The forces at the endpoints of element A can be expressed as follows:

$$\begin{cases} \boldsymbol{F}_{A1} = \dfrac{\left|\overrightarrow{PA_2}\right|}{\left|\overrightarrow{A_1A_2}\right|}\boldsymbol{F}_A, \\ \boldsymbol{F}_{A2} = \left(1 - \dfrac{\left|\overrightarrow{PA_2}\right|}{\left|\overrightarrow{A_1A_2}\right|}\right)\boldsymbol{F}_A. \end{cases} \tag{10}$$

According to Newton's third law, the contact force on the ring is $\boldsymbol{F}_{ring} = F\boldsymbol{e}_{PQ}$. Given that the ring is fixed on the edge of the net and its size is much smaller than that of the net, the following assumptions are made to simplify the dynamics model. The center of mass of the ring is fixed on the midpoint of the element of the net. The normal vector of the ring is always parallel to the element and cannot slide or rotate relative to the element. According to these assumptions, the contact forces on the ring are superimposed on the center of mass of the ring, and the torque generated by the contact force on the ring is not considered. If ring B collides with more than one element simultaneously, then the forces at ring B can be expressed as follows:

$$\boldsymbol{F}_{ring} = \sum_{i=1}^{n} \boldsymbol{F}_{ring,i}, \tag{11}$$

where n is the number of contacts occurring at the same time, $\boldsymbol{F}_{ring,i}$ is the contact force of the ring of the i-th contact. The ring attached to the net edge and element C indicates the piece of the thread that fixed the ring. The ring is located at the middle point of element C of the net and cannot slide or rotate relative to element C. Therefore, the contact force on the ring can be distributed to the endpoints of element C as follows:

$$\begin{cases} \boldsymbol{F}_{C1} = \dfrac{1}{2}\boldsymbol{F}_{ring}, \\ \boldsymbol{F}_{C2} = \dfrac{1}{2}\boldsymbol{F}_{ring}. \end{cases} \tag{12}$$

5. Simulation Results and Validation

For the thread-ring sliding joint presented in this study, the closing thread is discretized into a series of nonbending elements. When the number of elements discretized by the closing thread is too small, the thread cannot fit the curved surface of the ring completely, so the thread and the ring cannot slide normally. Therefore, discretizing the thread into adequate elements is necessary to ensure the relative slip between thread and ring. In this section, the discrete number of the closing thread will be obtained through the simulations of the thread pulling a ring. A one-edge closure experiment of the net is carried out, and the experimental results are compared with the simulation results. Moreover, the entire process of deployment and closure of a net will be simulated to demonstrate the performance of the split closing mechanism. In this study, the friction between the net and the target is not considered, as well as the friction between the closing thread and the ring. The collision between the net and the closing thread and the self-collision of the net are not considered.

5.1. Simulations of a Thread Pulling a Ring. The simulations of pulling a ring are studied to determine the optimal number of elements. A ring is placed at the origin of the coordinate with a normal vector pointing to the Y-axis and constrained to move along the Y-axis. A one-meter long thread is passed through the ring and placed parallel to the Y-axis; its starting point is $[0, -0.2, 0]$ m, and the endpoint is fixed at $[0, 0.8, 0]$ m. The starting point of the thread is connected to a ball with a mass of 0.1 kg. The ball has an initial velocity of $[0, 0, -1]$ m/s. Figure 6 shows the initial state of the simulation, and Table 1 shows the simulation parameters.

Figure 7 illustrates the simulation results by the mass-spring-damper method and ABAQUS. In ABAQUS, the truss element is used to model the thread, and the general contact is used between the thread and ring. For easy observation, the ring in Figure 7 is enlarged. It can be found that the simulation results of the two methods are in good agreement. The ball has a velocity towards the negative direction of Z-axis; it drives the thread away from the axis of $Z = 0$. When the thread is in contact with the ring, the ring goes forward along the Y-axis under contact force. The ball eventually passes the ring in the positive direction of the Y-axis and continues to drag it.

Figure 8 presents the Y-displacement of the mass-spring-damper method with different element numbers and the Y-displacement obtained by the ABAQUS method. Simulation with 100, 200, and 300 elements takes 5.2, 10.1, and 15.4 minutes, respectively. The displacement curve of the ring is smooth without abrupt changes, which verifies the feasibility of the thread-ring sliding joint. When the number of elements is more than 200, the time-displacement curves almost coincide. When the number of elements is less than 200, the displacement of the ring is larger after $t = 0.8$ s. The higher the number of elements is, the smoother the slip between the thread and the ring is. At the same time, we also find that the displacement curve obtained by ABAQUS is the closest to that when the number of elements is 200. Therefore, a 1 m long thread can be discretized into 200 elements to obtain a high calculation efficiency. Figure 9 shows the maximum contact force of the ring with a different number of elements. The larger the number of elements is, the smaller the maximum contact force on the ring is.

5.2. One-Edge Closure Experiment and Simulation. To validate the thread-ring sliding model proposed in this study, a one-edge closure experiment of the net is carried out and the experimental results are compared with the simulation results. Figure 10 illustrates a comparison diagram between the experiment and simulation results. The simulation takes approximately 55.1 minutes. Figure 10(a) shows the experiment scenario and simulation of the net at the initial state. Two corners of the upper edge of the net are fixed on the experiment platform constructed by aluminum profiles and the net hanging naturally under gravity. The four rings are fixed on the lower edge of the net at the positions shown in Figure 4. The closing thread pass through four rings, and two 0.1 kg masses are fixed at the ends of the closing thread. Due to the fabrication error of the net, the distance between the center point of the lower net edge and the mass on the left side is about 0.585 m. The simulation is modeled according to this distance. The experimental and simulation parameters are shown in Table 2.

After the electromagnet is turned off at 0 s, the masses will fall under gravity. From 0 s to 0.5 s, the masses gradually fall and drive the closing thread to slide relative to the ring, and the lower net edge bunched up gradually. It can be found that the simulation has a good agreement with the experiment results. Due to the initial position deviation of the closing thread, the mass on the left side is lightly higher than the mass on the right side in the vertical direction at 0.5 s. The two masses contact at about 0.5 s, but there is no collision detection for the masses in the simulation. Therefore, the movement state of the closing thread in the experiment is a little different from that in the simulation as seen in Figure 10(g). However, the lower net edge in both the experiment and simulation has been completely bunched up.

5.3. Net Closure Simulations. In the following simulations, the thread-ring sliding joint is used to simulate the closing process. The performance of the closing mechanism proposed in Section 2 is demonstrated. Figure 4 shows the configuration of the net and the closing system.

The net is stored at the origin of the coordinate. The velocity of the closing mechanisms shot by the chaser spacecraft is set to 1 m/s with an angle of 35° to the Z-axis. The center of a ball target is fixed at $[0, 0, 1]$ m with a radius of 0.15 m. The starting time of closing is 1.5 s, and before closure, the closing threads coincide entirely with the edge of the net. During the deployment, the rings and the closing threads do not slide relatively, and they have little influence on the deployment process, so when simulating this stage, the mass of the rings and the closing threads has been superimposed on the nodes of the net edges before the closure, and there is no collision detection between the rings and the closing threads until the closure begins. Table 3 shows the separation velocity of the split masses of the closing mechanism when the starting time of closing is reached. Table 4 shows the simulation parameters, and the parameters of the closing thread and the ring are shown in Table 1. This simulation takes approximately 116.5 minutes.

Figure 11 illustrates the process of deployment and closure of the net. In the first 3 screenshots of Figure 11, the pink ball indicates the closing mechanism, which is not activated during this period, the split masses and the launcher can be regarded as a whole with a mass of 0.25 kg. After the closing mechanism is activated, the green ball represents the split mass with a mass of 0.1 kg, and the pink ball no longer represents the whole closing mechanism, but only the launcher, with a mass of 0.05 kg. The net deploys gradually and collides with the ball at approximately $t = 1.45$ s. The starting time of closing is set to $t = 1.5$ s. At $t = 1.6$ s, it can be seen that the split masses have split from each other and drive the closing thread to move with it. At this time, the closing threads and the rings have not slipped obviously, and the shape of the net has not considerably changed. After $t = 1.6$ s, the pulling tendency of the closing threads to the rings changes to the relative sliding between them. The length of the closing threads increases gradually from $t = 1.7$ s to $t = 1.8$ s, due to the pulling of the split masses. The launchers are closing to each other, and the area of the net mouth decreases gradually. At $t = 1.9$ s, the net mouth is closed completely, and the target is wrapped totally.

Figure 12 shows the X, Y, and Z velocities of split masses A and B of closing mechanism 1. The closure begins at 1.5 s. The velocity of split masses A and B on X-axis and Y-axis shows a jump of 2 m/s, and the directions are consistent with

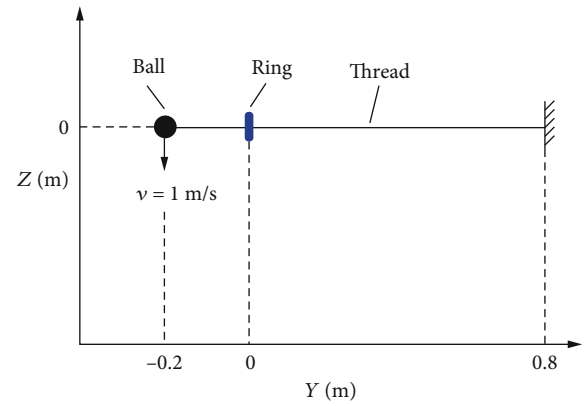

Figure 6: Initial state of the simulation.

Table 1: Simulation parameters.

Parameter	Value
Thread length (m)	1
Number of elements	200
Thread Young's modulus (GPa)	1
Thread Poisson's ratio	0.3
Thread density (kg/m^3)	970
Thread diameter (m)	0.002
Ball mass (kg)	0.1
Ring diameter (m)	0.02
Ring wire diameter (m)	0.004
Ring mass (kg)	0.1
Ring Young's modulus (GPa)	70
Ring Poisson's ratio	0.33

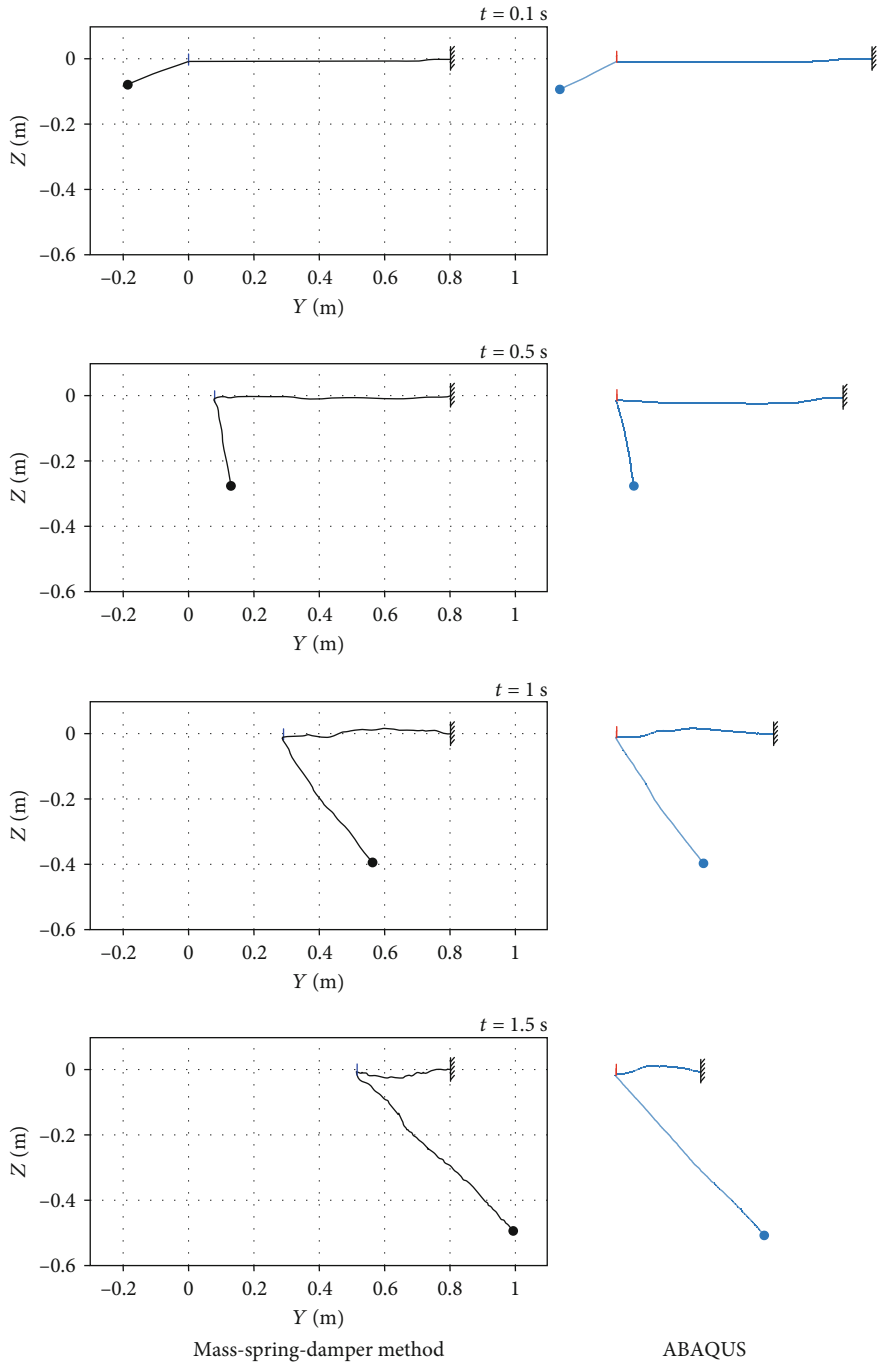

Figure 7: Comparison of simulation results.

the separation velocity shown in Table 2. The velocity on Z -axis has no abrupt change due to the absence of separation velocity. The change of velocity of the two split masses is symmetrical, which is also in line with the setting of the same mass, the same separation speed, and the opposite direction of the two split masses in Section 2. Taking the split mass A as an example, its velocity on -axis is perpendicular to the normal vector of ring 16. The resistance is substantial after the beginning of closure. Therefore, a substantial velocity attenuation occurs from $t = 1.5$ s to $t = 1.6$ s, and the kinetic energy of the split mass is converted into the elastic potential energy of the closing thread and the net. After $t = 1.6$ s, with the closing of the net, the velocity on X-axis gradually increases and the velocity turns to the positive direction of X-axis. This process can also be observed in Figure 11. The velocity on Y-axis of the split mass A is parallel to the normal vector direction of ring 16. It suffers less resistance, hence, its velocity has less reduce from $t = 1.5$ s to $t = 2$ s.

Figure 13 reveals the contact force on rings 1 and 2. Ring 1 collides with the closing thread at 1.503 s with a contact force of approximately 37 N. Ring 2 collides with the closing thread at 1.509 s with a contact force of approximately 8.1 N.

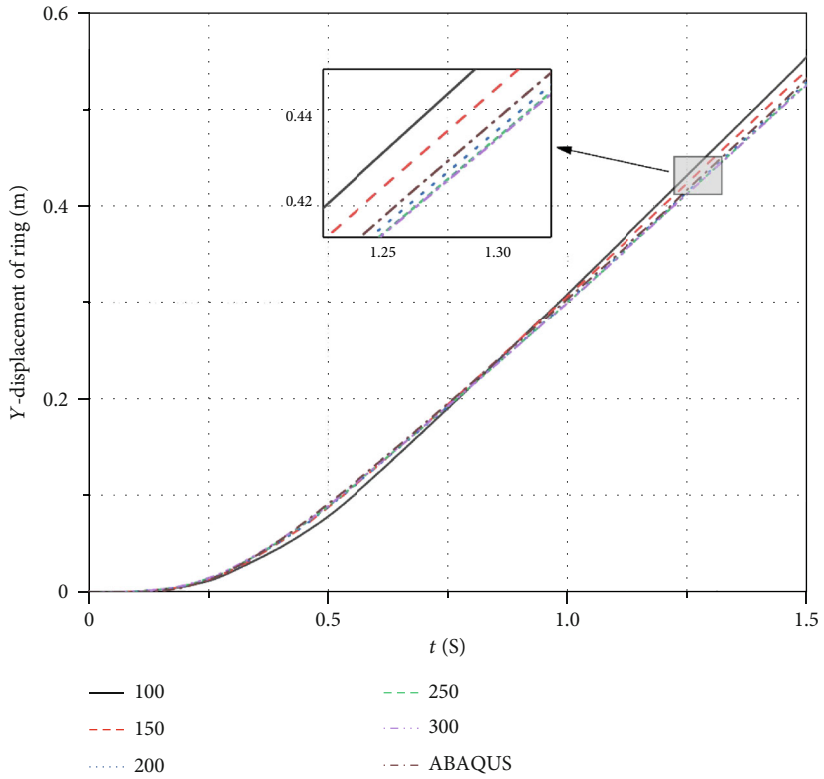

Figure 8: Displacement of the ring on Y-axis.

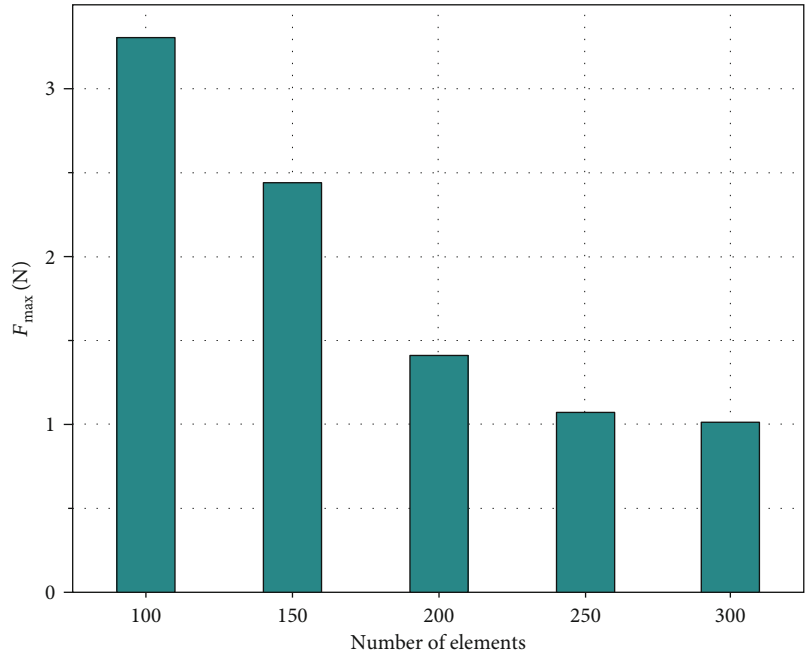

Figure 9: Maximum contact force of the ring.

Figure 13(a) shows that a wave crest occurs at approximately $t = 1.6$ s, and the force on ring 1 reaches its maximum value. This observation is consistent with the phenomenon shown in Figure 12 that the pulling trend of the closing thread to the ring after 1.6 s has changed to the sliding between them. At $t = 1.9$ s, the closure is completed, and the closing thread produces a substantial force on ring 2, as shown in Figure 13(b).

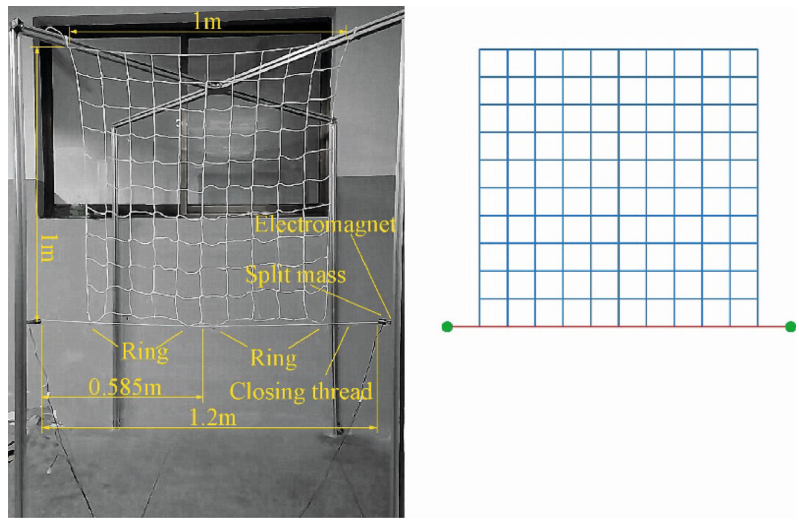

(a) $t = 0$ s

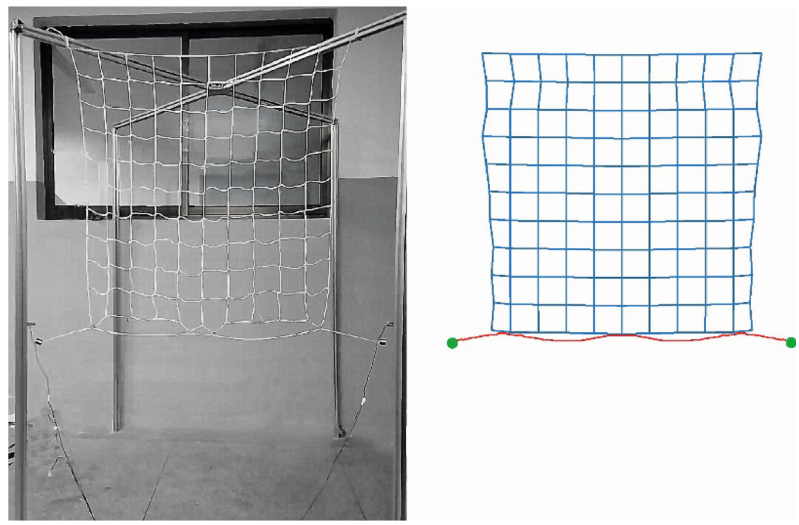

(b) $t = 0.1$ s

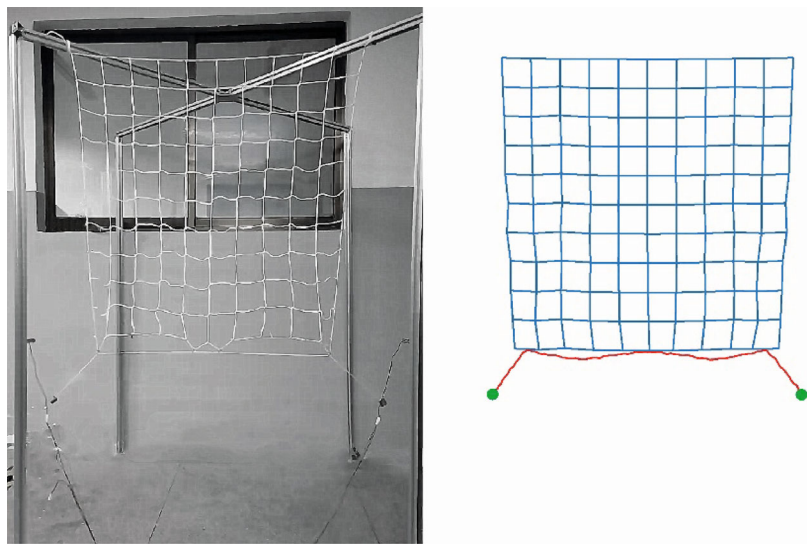

(c) $t = 0.2$ s

Figure 10: Continued.

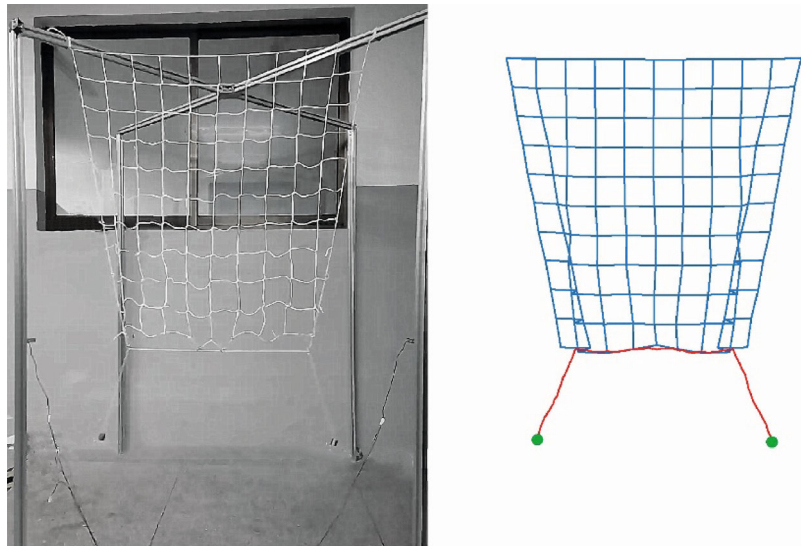

(d) $t = 0.3$ s

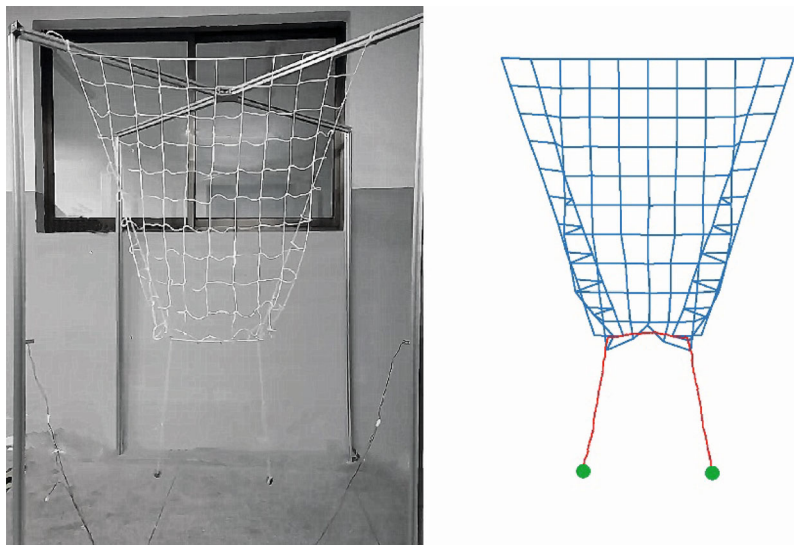

(e) $t = 0.4$ s

Figure 10: Continued.

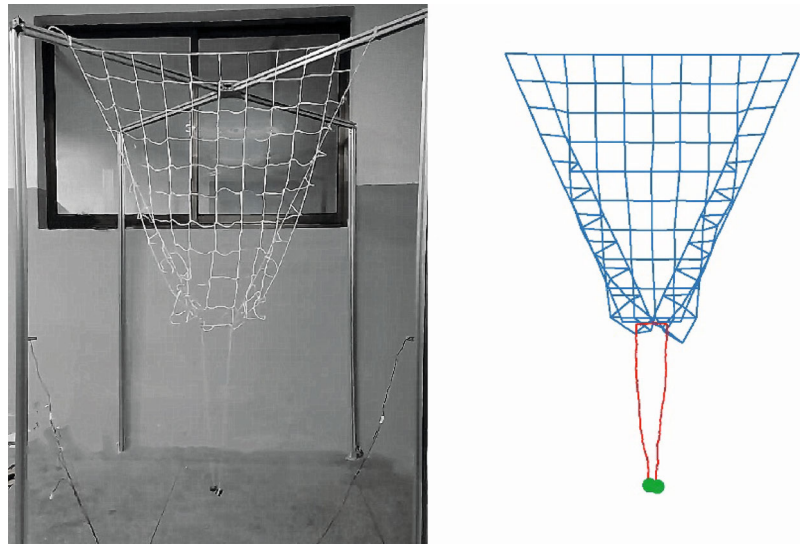

(f) $t = 0.5$ s

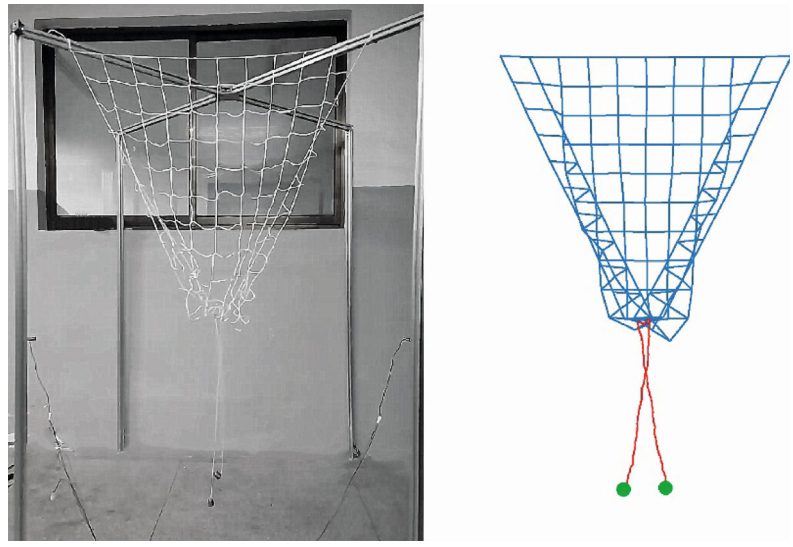

(g) $t = 0.55$ s

Figure 10: One-edge closure experiment and simulation.

Table 2: Experimental and simulation parameters.

Parameter	Value
Thread Young's modulus (GPa)	87
Thread Poisson's ratio	0.35
Thread density (kg/m^3)	650
Net size (m^2)	1×1
Net mesh (m)	0.1
Thread diameter (m)	0.002
Closing thread length (m)	1.2
Element number of closing thread	240
Ring mass (kg)	0.001
Ring diameter (m)	0.014
Ring wire diameter (m)	0.002

To demonstrate the performance of the split closing mechanism, the closing process of the net with different starting times of closing is simulated. The starting time of closing is set to 1.2 s, 1.3 s, 1.4 s, 1.5 s, and 1.6 s, and the images of the five cases are obtained after 0.4 s of the starting time of closing, as shown in Figure 14. Even if the span of the starting time of closing of different cases is 0.4 s, the net mouth can be closed completely, and the target can be wrapped reliably. Given that the net contacts with the target at approximately 1.45 s, the closing mechanism can make the tether-net closing successfully, whether it starts to work before or after the net contacts with the target. Moreover, the later the closure begins, the farther the split masses move forward on the positive direction of Z-axis.

All the simulations in this paper are implemented in Visual C++, and the ordinary differential equations in Section 3 are solved via the central difference method. All the

Table 3: Separation velocity of the split masses.

	Split mass A	Split mass B
Closing mechanism 1	[−2,−2, 0] m/s	[2, 2, 0] m/s
Closing mechanism 2	[−2, 2, 0] m/s	[2,−2, 0] m/s
Closing mechanism 3	[2, 2, 0] m/s	[−2,−2, 0] m/s
Closing mechanism 4	[2,−2, 0] m/s	[−2, 2, 0] m/s

Table 4: Simulation parameters.

Parameter	Value
Thread Young's modulus (GPa)	87
Thread Poisson's ratio	0.35
Thread density (kg/m^3)	970
Net size (m^2)	1×1
Net mesh (m)	0.1
Thread diameter (m)	0.002
Closing thread length (m)	1.2
Element number of closing thread	240
Closing mechanism mass (kg)	0.25
Ring mass (kg)	0.006
Mass of split mass (kg)	0.1
Target Young's modulus (GPa)	2.3
Target Poisson's ratio	0.39

simulations are performed on a laptop with Intel Core i7-6700HQ CPU at 2.60 GHz. In this study, the simulations include a large number of elements and collision detection and use a small time step of 1×10^{-6} s, so the simulation time of net closure looks not short.

6. Conclusions

In this study, the dynamics model of the split closing mechanism and the thread-ring sliding joint are explored. The dynamics model of a quadrilateral net with square mesh is established based on the mass-spring-damper method. A split closing mechanism is proposed for the first time, which drives the closing thread to close the net by launching two split masses with the same mass and speed. For the first time, the model of a thread-ring sliding joint is proposed based on the mass-spring-damper method, which can be used to simulate the closing process of tether-net. The golden section method is used to search the minimum distance between the closing thread and the ring. A nonlinear damping model is used to calculate the contact force when the minimum distance satisfies the collision condition.

The current work reveals that the thread-ring sliding joint can be used to simulate the relative slip between the thread and the ring. A 1 m long thread is suggested to be discretized into 200 elements to obtain stable results and higher calculation efficiency. In collision detection, the flexible thread is discretized into a series of nonbendable cylinders. Thus, the thread cannot fit the curved surface of the ring entirely, which is the limitation of this model. However, macroscopically, this does not affect the relative slip between the thread and the ring, and no drop or penetration occurs between the thread and the ring. The simulation results of

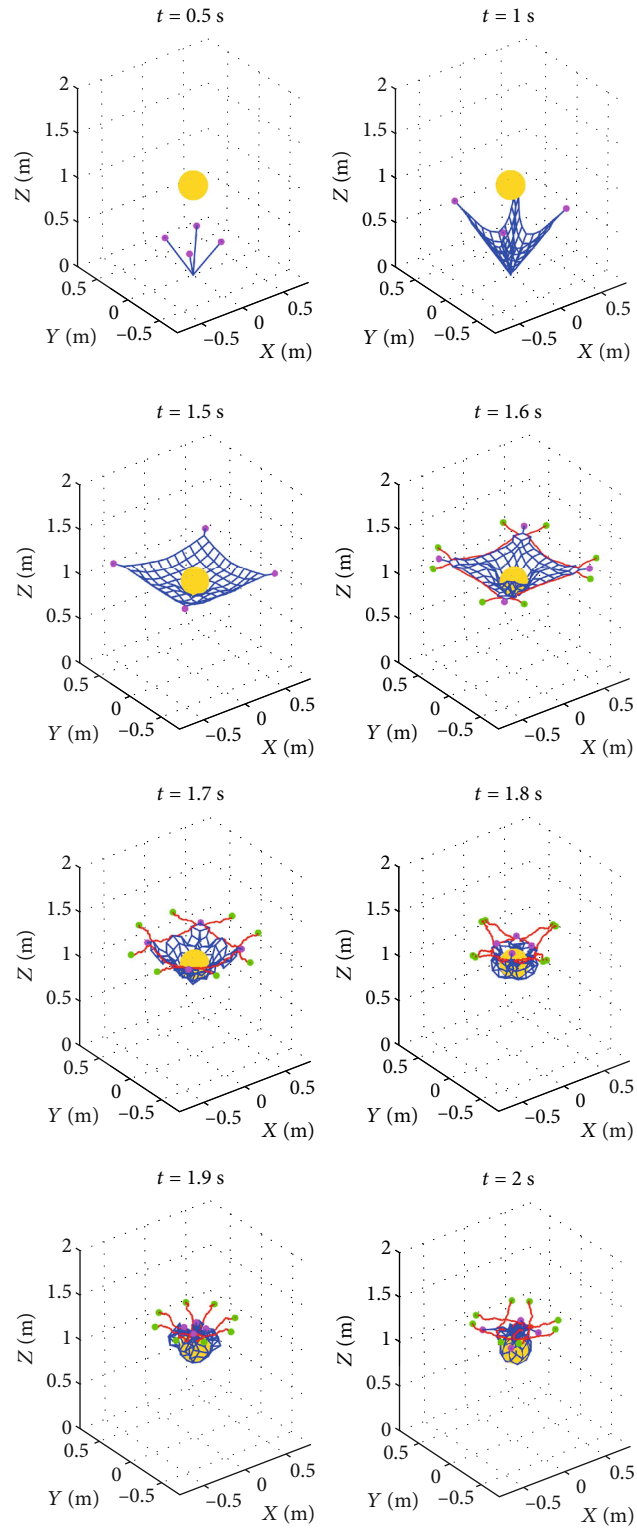

Figure 11: Closure sequence of the net.

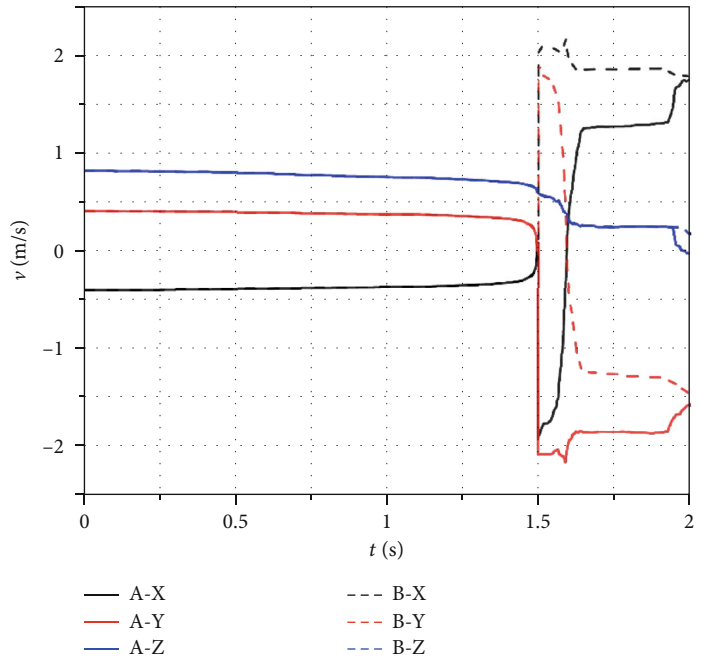

Figure 12: X, Y, and Z velocities of split masses A and B of closing mechanism 1.

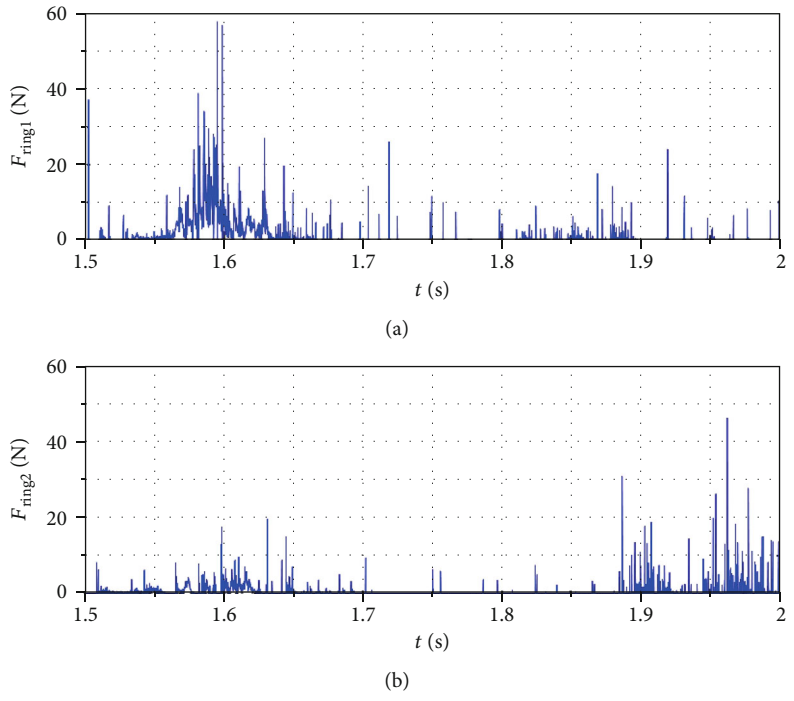

Figure 13: Contact force on rings 1 and 2.

one-edge closing of the net is in good agreement with the experimental results, which verifies the thread-ring sliding model.

The tether-net can wrap the target reliably in a short time by using the split closing mechanism. The split closing mechanism can make the tether-net closing successfully, whether it starts to work before or after the net contacts with the target. By replacing the separate power of the closing mechanism, the closing mechanism has the capacity to implement the capture task of tether-net with different sizes.

In real ADR scenarios, many complex situations may occur, such as inconsistent launching angle of the closing mechanism and winding or jamming of closing threads. The impact of these problems on closure needs to be

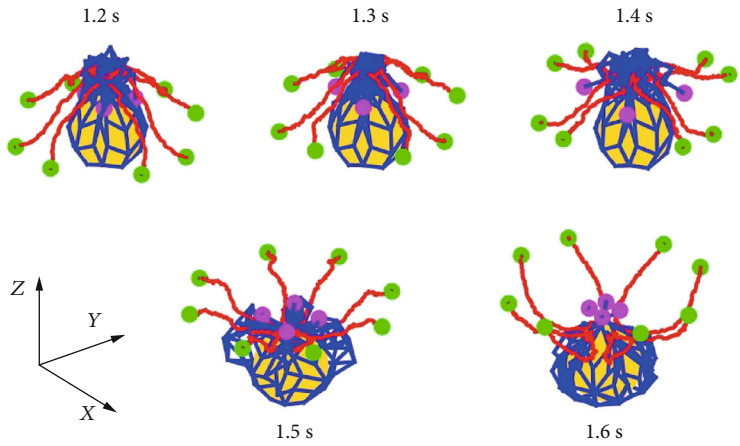

Figure 14: Five cases with different starting times of closing.

evaluated. Therefore, in future works, we will focus on parameter sensitivity analysis of closure and capture probability of the tether-net.

Data Availability

Data will be available on reasonable request.

Conflicts of Interest

The authors declare that they have no conflicts of interest.

Acknowledgments

This work was supported in part by the National Natural Science Foundation of China (Grant 11802130), the Natural Science Foundation of Jiangsu Province (Grant BK20170819), and the Postgraduate Research & Practice Innovation Program of Jiangsu Province.

References

[1] J. N. Pelton, *New Solutions for the Space Debris Problem*, Springer International Publishing, Cham, 2015.

[2] M. Shan, J. Guo, and E. Gill, "Review and comparison of active space debris capturing and removal methods," *Progress in Aerospace Sciences*, vol. 80, pp. 18–32, 2016.

[3] P. Huang, F. Zhang, L. Chen et al., "A review of space tether in new applications," *Nonlinear Dynamics*, vol. 94, no. 1, pp. 1–19, 2018.

[4] J. Si, Z. Pang, Z. Du, and C. Cheng, "Dynamics modeling and simulation of self-collision of tether-net for space debris removal," *Advances in Space Research*, vol. 64, no. 9, pp. 1675–1687, 2019.

[5] R. Benvenuto, M. Lavagna, and S. Salvi, "Multibody dynamics driving GNC and system design in tethered nets for active debris removal," *Advances in Space Research*, vol. 58, no. 1, pp. 45–63, 2016.

[6] M. Shan, J. Guo, and E. Gill, "Deployment dynamics of tethered-net for space debris removal," *Acta Astronautica*, vol. 132, pp. 293–302, 2017.

[7] M. Shan, J. Guo, E. Gill, and W. Gołębiowski, "Validation of space net deployment modeling methods using parabolic flight experiment," *Dynamics*, vol. 40, no. 12, pp. 3319–3327, 2017.

[8] M. Shan, J. Guo, and E. Gill, "Contact dynamic models of space debris capturing using a net," *Acta Astronautica*, vol. 158, pp. 198–205, 2019.

[9] E. M. Botta, I. Sharf, A. K. Misra, and M. Teichmann, "On the simulation of tether-nets for space debris capture with vortex dynamics," *Acta Astronautica*, vol. 123, pp. 91–102, 2016.

[10] E. M. Botta, I. Sharf, and A. K. Misra, "Contact dynamics modeling and simulation of tether nets for space-debris capture," *Journal of Guidance, Control, and Dynamics*, vol. 40, no. 1, pp. 110–123, 2017.

[11] J. L. Forshaw, G. S. Aglietti, N. Navarathinam et al., "RemoveDEBRIS: an in-orbit active debris removal demonstration mission," *Acta Astronautica*, vol. 127, pp. 448–463, 2016.

[12] L. Cercós, R. Stefanescu, A. Medina et al., "Validation of a net active debris removal simulator within parabolic flight experiment," in *12th International Symposium on Artificial Intelligence, Robotics and Automation in Space*, pp. 17–19, Montreal, Canada, 2014.

[13] R. Axthelm, B. Klotz, I. Retat, U. Schlossstein, W. Tritsch, and S. Vahsen, "Net capture mechanism for debris removal demonstration mission," in *Proceedings of the 7th European Conference on Space Debris*, pp. 18–21, Darmstadt, Germany, June 2017.

[14] F. Zhang and P. Huang, "Releasing dynamics and stability control of maneuverable tethered space net," *IEEE/ASME Transactions on Mechatronics*, vol. 22, no. 2, pp. 983–993, 2017.

[15] P. Huang, F. Zhang, J. Cai, D. Wang, Z. Meng, and J. Guo, "Dexterous tethered space robot: design, measurement, control, and experiment," *IEEE Transactions on Aerospace and Electronic Systems*, vol. 53, no. 3, pp. 1452–1468, 2017.

[16] R. Benvenuto, S. Salvi, and M. Lavagna, "Dynamics analysis and GNC design of flexible systems for space debris active removal," *Acta Astronautica*, vol. 110, pp. 247–265, 2015.

[17] G. Hausmann, M. Wieser, R. Haarmann et al., "E. Deorbit mission: OHB debris removal concepts," in *Proceeding of the 13th Symposium on Advanced Space Technologies in Robotics and Automation (ASTRA'2015)*, Noordwijk, Niederlande, May 2015.

[18] G. Zhai and J. Zhang, "Space tether net system for debris capture and removal," in *2012 4th International Conference on Intelligent Human-Machine Systems and Cybernetics*, pp. 257–261, Nanchang, China, August 2012.

[19] I. Sharf, B. Thomsen, E. M. Botta, and A. K. Misra, "Experiments and simulation of a net closing mechanism for tether-net capture of space debris," *Acta Astronautica*, vol. 139, pp. 332–343, 2017.

[20] E. M. Botta, C. Miles, and I. Sharf, "Simulation and tension control of a tether-actuated closing mechanism for net- based capture of space debris," *Acta Astronautica*, vol. 174, pp. 347–358, 2020.

[21] A. Collina and S. Bruni, "Numerical simulation of pantograph-overhead equipment interaction," *Vehicle System Dynamics*, vol. 38, no. 4, pp. 261–291, 2002.

[22] J.-H. Seo, S.-W. Kim, I.-H. Jung et al., "Dynamic analysis of a pantograph–catenary system using absolute nodal coordinates," *Vehicle System Dynamics*, vol. 44, no. 8, pp. 615–630, 2006.

[23] M. Lesser, L. Karlsson, and L. Drugge, "An interactive model of a pantograph-catenary system," *Vehicle System Dynamics*, vol. 25, pp. 397–412, 1996.

[24] A. A. Shabana, "An absolute nodal coordinate formulation for the large rotation and large deformation analysis of flexible bodies," Techn. Rep. No. MBS96–1-UIC, University of Illinois at Chicago, Chicago, IL, USA, 1996.

[25] A. A. Shabana, *Computational Continuum Mechanics*, John Wiley & Sons, New York, NY, USA, 2018.

[26] J. Gerstmayr and A. A. Shabana, "Analysis of thin beams and cables using the absolute nodal co-ordinate formulation," *Nonlinear Dynamics*, vol. 45, no. 1-2, pp. 109–130, 2006.

[27] D. Vranek, "Fast and accurate circle-circle and circle-line 3D distance computation," *Journal of Graphics Tools*, vol. 7, no. 1, pp. 23–31, 2002.

[28] D. H. Eberly, *3D Game Engine Design: A Practical Approach to Real-Time Computer Graphics*, CRC Press, 2006.

[29] P. Venkataraman, *Applied Optimization with MATLAB Programming*, John Wiley & Sons, 2009.

[30] J. A. Koupaei, S. M. M. Hosseini, and F. M. M. Ghaini, "A new optimization algorithm based on chaotic maps and golden section search method," *Engineering Applications of Artificial Intelligence*, vol. 50, pp. 201–214, 2016.

[31] K. H. Hunt and F. R. E. Crossley, "Coefficient of restitution interpreted as damping in vibroimpact," *Journal of Applied Mechanics*, vol. 42, no. 2, pp. 440–445, 1975.

[32] K. L. Johnson, *Contact Mechanics*, Cambridge University Press, 1987.